Available online at www.sciencedirect.com
SCIENCE DIRECT®
Journal of Chromatography A, 1035 (2004) 177–193
JOURNAL OF CHROMATOGRAPHY A
www.elsevier.com/locate/chroma

# Chromatographic impulse response technique with curve fitting to measure binary diffusion coefficients and retention factors using polymer-coated capillary columns

Chang Yi Kong [a,*], Toshitaka Funazukuri [b], Seiichiro Kagei [a]

[a] *Faculty of Environment and Information Sciences, Yokohama National University, 79-7 Tokiwadai, Hodogaya-ku, Yokohama 240-8501, Japan*
[b] *Department of Applied Chemistry, Institute of Science and Engineering, Chuo University, 1-13-27 Kasuga, Bunkyo-ku, Tokyo 112-8551, Japan*

Received 28 August 2003; received in revised form 17 February 2004; accepted 18 February 2004

**Abstract**

The theoretical basis of a Gaussian-like approximate solution was applied to a chromatographic impulse response technique with curve fitting for measuring binary diffusion coefficients and retention factors using a polymer-coated capillary column. The formulae were derived for evaluating both the accuracy of the approximate solution and the sensitivity of the parameters. The validity of the solution also was confirmed experimentally for pulse injection of phenol in acetone into supercritical carbon dioxide flowing at 313.15 K and 11.6–28.6 MPa. Potential sources for experimental errors of the method are discussed.


*Keywords:* Impulse response technique; Curve fitting; Binary diffusion coefficient; Retention factor; Mathematical modeling; Transient response

## 1. Introduction

Transient response techniques have been employed for determining transport properties of fluids such as diffusion coefficients and thermal conductivities. Binary diffusion coefficients in supercritical fluids were measured mainly by the Taylor dispersion method [1,2], which is a type of impulse response technique. Although a large number of studies on binary diffusion coefficients in supercritical carbon dioxide have been reported (refer to [3,4]), few data exist for useful compounds with relatively high molecular weights.

A low viscous liquid, i.e., low molecular weight compound, can be easily input as a pulse into a solvent stream through an ordinary HPLC injector. However, highly viscous or solid solutes, which often have relatively high molecular weights, are difficult to inject. Thus, the solute is injected as a solution in a supercritical fluid [5–14] or other solvent (such as hexane [15,16] and isooctane [17]) having essentially no UV absorption because a UV detector is commonly employed. Both choices possess some drawbacks: adjusting the amount of the input solute is difficult in the former case, and the effect of the dissolving solvent on diffusion coefficients is not clear in the latter case. When a capillary column coated with a polymer film on the inner wall is employed, a certain amount of highly viscous liquid or a solid solute dissolved in an organic solvent can be loaded. Since the solute and organic solvent are chromatographically separated in the column, the effect of the solvent can be eliminated.

Lai and Tan [18] employed a polymer-coated diffusion column for the measurements of binary diffusion coefficients and retention factors, which were analyzed by the moment method. While this method does not require the analytical solution of the fundamental differential equation in Eq. (1), it has been noted that small errors in the frontal and the tailing portions of the response signals are unduly weighted (refer to [19]). Moreover, the validity of the model cannot be judged by this method because the degree of the fit of the calculated response curve to that measured experimentally cannot be evaluated directly. Although the curve-fitting method overcomes these drawbacks, it requires analytical expression of the response curve.

For linear and equilibrium adsorption occurring on and/or in a polymer film coated on the column wall, Golay [20] derived an approximate equation for cross-sectional average concentration based on the quadratic profile in the column. Funazukuri et al. [21,22] have determined infinite-dilution

* Corresponding author. Tel.: +81-45-339-4396; fax: +81-45-339-4396.
*E-mail address:* kong@ynu.ac.jp (C.Y. Kong).

0021-9673/$ – see front matter © 2004 Elsevier B.V. All rights reserved.
doi:10.1016/j.chroma.2004.02.067

binary diffusion coefficients and retention factors for highly viscous and solid compounds in supercritical carbon dioxide with a Gaussian-like approximate solution [23].

The severe distortion and/or tailing of the response curves, mainly caused by the strong solute polarity, cannot be represented by the Gaussian-like approximate solution to a linear and equilibrium adsorption isotherm. Although Madras et al. [24] have determined from numerical calculations that non-equilibrium adsorption causes tailing of response curves in the Taylor dispersion measurements, tailing for most solutes, except for those strong polar compounds such as solutes with carboxyl groups, is not significant with a polymer-coated capillary column. Thus, we can assume that the partitioning of a solute between the polymer and the supercritical phases behaves as a linear and equilibrium adsorption isotherm unless the solute is strongly polar and/or unless the concentration is high.

As mentioned earlier, the impulse response method with a polymer-coated capillary column is amenable to measurement of binary diffusion coefficients and retention factors for various solutes having low to medium polarity over a wide range of molecular weights. This method is applicable to the analysis of transport phenomena in various thermodynamic measurements and to processes involving chemical reactions and separations such as supercritical fluid extraction and chromatography. However, the theoretical basis is not well understood. Thus, our objective is to provide a theoretical basis for the curve-fitting method when determining binary diffusion coefficients and retention factors from impulse response measurements with a polymer-coated capillary column. In addition, we demonstrate experimentally the validity of this method. From a single injection of a solid solute dissolved in an organic solvent (for example, phenol in acetone), the simultaneous determination of binary diffusion coefficient and retention factor was accomplished for both solute and solvent. Finally, we examine the effects of the solvent (acetone) on parameters of the solute (phenol) by multiple injections of the solvent soon after loading the tracer solution into the diffusion column.

## 2. Prediction of impulse response curve

### 2.1. Linear adsorption model

When a tracer component is pulse-injected into a fully developed laminar flow in a cylindrical column, and the assumption that the physical properties are constant during each measurement can be made, the tracer concentration $c(r, \phi, x, t)$ is described as [2,25]:

$$\frac{\partial c}{\partial t} = D_{12}\left\{\frac{1}{r}\frac{\partial}{\partial r}\left(r\frac{\partial c}{\partial r}\right) + \frac{1}{r^2}\frac{\partial^2 c}{\partial \phi^2} + \frac{\partial^2 c}{\partial x^2}\right\} - 2u_a\left\{1-\left(\frac{r}{R}\right)^2\right\}\frac{\partial c}{\partial x} \quad (1)$$

$$\frac{\partial c}{\partial r} = \text{finite} \quad \text{at } r = 0 \quad (2)$$

$$c = 0 \quad \text{at } x = \pm\infty \quad (3)$$

where $D_{12}$ is the binary diffusion coefficient of the tracer component in the fluid, $R$ the column radius, $u_a$ the average fluid velocity, $t$ the time, and $r$, $\phi$ and $x$ the radial, angular and axial variables, respectively. On the inner wall coated with an adsorbent, the following boundary condition is given with the assumption that an adsorption isotherm is linear and the tracer component instantaneously reaches equilibrium between the fluid and adsorbent on the wall:

$$k\frac{\partial c}{\partial t} = -\frac{2D_{12}}{R}\frac{\partial c}{\partial r} \quad \text{at } r = R \quad (4)$$

where $k$ is the retention factor, also called the partition ratio or capacity factor. Assuming that the tracer component attains equilibrium on the wall at $t = 0$, initial condition for the pulse input can be written as:

$$c = \left(\frac{m}{\pi R^2}\right)\frac{\delta(x)}{1+k} \quad \text{at } t = 0 \quad (5)$$

where $m$ is the injected amount of tracer.

According to the symmetric concentration profile around the $x$-axis for initial condition of Eq. (5), $c$ is a function of $r$, $x$ and $t$. Although $\phi$ is eliminated later, the inclusion of $\phi$ at this point is practical.

In most experiments, average concentration over the cross-section of a column is measured by a UV detector. $C$ is the cross-sectional average concentration:

$$C(x, t) = \frac{2}{R^2}\int_0^R c(r, x, t) r\,\mathrm{d}r \quad (6)$$

We call this model the cylindrical model. Because it is difficult to obtain the analytical expression for $C$, we derive an approximate solution for $C$ in Section 2.2.

### 2.2. Gaussian-like approximate solution

By assuming that $|c(r, x, t) - C(x, t)| \ll C(x, t)$, Golay [20] derived an approximate equation for $C$ from Eqs. (1), (2) and (4):

$$\frac{\partial C_G}{\partial t} = a\frac{\partial^2 C_G}{\partial z^2} - b\frac{\partial^2 C_G}{\partial z\,\partial t} \quad (7)$$

where

$$a = \frac{D_{12}}{1+k} + \frac{1+6k+11k^2}{1+k}\frac{R^2U^2}{48D_{12}} \quad (7a)$$

$$b = \frac{k(1+4k)}{1+k}\frac{R^2U}{24D_{12}} \quad (7b)$$

$$z = x - Ut \quad (7c)$$

$$U = \frac{u_a}{1+k} \quad (7d)$$

It should be noted that the second term of Eq. (7a) is dominant. If the first term is significant, we need not make measurements in a flowing system. Therefore, in this paper, we consider the following condition:

$$(1 + 6k + 11k^2)\frac{R^2U^2}{48{D_{12}}^2} \gg 1 \tag{8}$$

Practically, this assumption is valid for supercritical and liquid solvents.

For $b = 0$, we obtain the following approximate equations for $C$:

$$\frac{\partial C_{\mathrm{app}}}{\partial t} = a\frac{\partial^2 C_{\mathrm{app}}}{\partial z^2} \tag{9}$$

$$C_{\mathrm{app}} = 0 \quad \text{at } z = \pm\infty \tag{10}$$

$$C_{\mathrm{app}} = \left(\frac{m}{\pi R^2}\right)\frac{\delta(z)}{1+k} \quad \text{at } t = 0 \tag{11}$$

Eqs. (9)–(11) can be solved as:

$$C_{\mathrm{app}}(x,t) = \left(\frac{m}{\pi R^2}\right)\frac{1}{(1+k)\sqrt{4\pi a t}}\exp\left\{-\frac{(x-Ut)^2}{4at}\right\} \quad \text{for } x, t > 0 \tag{12}$$

$C_{\mathrm{app}}$ is the Gaussian-like approximate solution. As discussed in Section 3, a simple analytical expression enables the theoretical evaluation of parameter sensitivity.

### 2.3. Accuracy of approximation

The validity of the approximation from $C$ to $C_{\mathrm{app}}$ can be examined by comparing spatial moments, as Aris [2] did for the Taylor dispersion. Using the space variable $z$ defined in Eq. (7c) instead of $x$, the $n$th spatial central moment of $c$ is defined as:

$$c^{(n)}(r,t) = \int_{-\infty}^{\infty} c(r,z,t)z^n \,\mathrm{d}z \tag{13}$$

The overall cross-sectional average concentration, $\bar{C}^{(n)}$, defined as the total amount of solute both in fluid and in polymer phase per cross-sectional area, is given by:

$$\bar{C}^{(n)}(t) = \frac{2}{R^2}\int_0^R c^{(n)}(r,t)r\,\mathrm{d}r + kc^{(n)}(R,t) \tag{14}$$

Then, the first and the second moments are given by Eqs. (15) and (16) (see Appendix A):

$$\bar{C}^{(1)}(t) = 0 \tag{15}$$

$$\frac{\bar{C}^{(2)}(t)}{\bar{C}^{(0)}} = 2at - \Gamma(t) \tag{16}$$

where

$$\Gamma(t) = \frac{1 + 8k + (97/4)k^2 + (57/2)k^3}{(1+k)^2}\frac{R^4U^2}{360{D_{12}}^2} - \frac{128(1+k)^2R^4U^2}{{D_{12}}^2}\sum_{n=1}^{\infty}\frac{\exp(-\lambda_n^2(D_{12}/R^2)t)}{\lambda_n^8\{1 + (k^2/(4(1+k)))\lambda_n^2\}} \tag{16a}$$

$\lambda_n$ is the $n$th positive root of the following equation:

$$2J_1(\lambda) + k\lambda J_0(\lambda) = 0 \tag{16b}$$

and $J_0(\lambda)$ and $J_1(\lambda)$ are the Bessel functions of the first kind of order 0 and 1, respectively.

On the other hand, the overall cross-sectional average of the Gaussian-like approximate solution, $\bar{C}_{\mathrm{app}}$, is given as:

$$\bar{C}_{\mathrm{app}}(x,t) = (1+k)C_{\mathrm{app}}(x,t) \tag{17}$$

Then, the first and the second spatial moments are:

$$\bar{C}_{\mathrm{app}}{}^{(1)}(t) = 0 \tag{18}$$

$$\frac{\bar{C}_{\mathrm{app}}{}^{(2)}(t)}{\bar{C}_{\mathrm{app}}{}^{(0)}} = 2at \tag{19}$$

Since the first terms in the RHS of Eqs. (16) and (19) are identical, the residual term in Eq. (16), $-\Gamma(t)$, can be considered as an index of the accuracy of $C_{\mathrm{app}}$. The second term in the RHS of Eq. (16a) is roughly approximated by the first term of the summation ($n = 1$). In fact, by defining $\Lambda(t)$ as:

$$\sum_{n=1}^{\infty}\frac{\exp(-\lambda_n^2(D_{12}/R^2)t)}{\lambda_n^8\{1 + (k^2/(4(1+k)))\lambda_n^2\}} \equiv \frac{\exp(-\lambda_1^2(D_{12}/R^2)t)}{\lambda_1^8\{1 + (k^2/(4(1+k)))\lambda_1^2\}}\Lambda(t) \tag{20}$$

$\Lambda(t)$ can be estimated as unity because:

$$1 < \Lambda(t) < 1 + \sum_{n=2}^{\infty}\frac{1}{(\lambda_n/\lambda_1)^8} \cong \sum_{n=1}^{\infty}\frac{1}{n^8} = \frac{\pi^8}{9450} \cong 1.0041 \tag{21}$$

Note that $\lambda_{0n} \le \lambda_1 \le \lambda_{1n}$, where $\lambda_{0n}$ and $\lambda_{1n}$ are the $n$th positive roots of $J_0(\lambda) = 0$ and $J_1(\lambda) = 0$, respectively. Fig. 1 shows $\lambda_1$ for various $k$ values. The second term in $\Gamma(t)$ usually is smaller than the first.

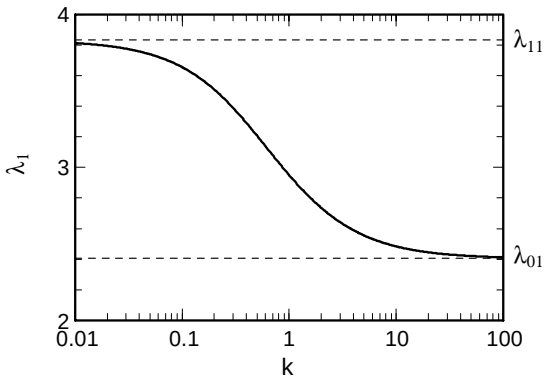


Fig. 1. $\lambda_1$ vs. $k$. Broken lines show $\lambda_{01} = 2.40483$ and $\lambda_{11} = 3.83171$, corresponding to the first positive zero points of $J_0(x)$ and $J_1(x)$, respectively.

Elimination of the residual terms in Eq. (16) is compensated for by changing the parameter values of the first term as $2(a + \Delta a)t$. Therefore,

$$\frac{\Delta a}{a} = -\frac{\Gamma(t)}{2at} \tag{22}$$

In Eq. (22), when $D_{12}$ varies and $k$ does not, eliminating the first term in Eq. (7a) provides:

$$\frac{\Delta D_{12}}{D_{12}} \cong \frac{\Gamma(t)}{2at} \tag{23}$$

## 3. Parameter determination by curve fitting

### 3.1. Curve fitting in the time domain

When relative fluid concentration is measured, the normalized concentration, $\hat{C}_{\mathrm{app}}$, which reduces the area equal to unity in the time interval $[t_1, t_2]$, is used. From Eq. (12) at $x = L$:

$$\hat{C}_{\mathrm{app}}(t) \equiv \frac{(1/\sqrt{4\pi at})\exp\{-(L-Ut)^2/(4at)\}}{\int_{t_1}^{t_2}(1/\sqrt{4\pi at})\exp\{-(L-Ut)^2/(4at)\}\mathrm{d}t} \tag{24}$$

Theoretically a whole time region $[0, \infty)$ may be used, which is represented by:

$$\hat{C}_{\mathrm{app}}(t) \equiv \frac{C_{\mathrm{app}}(L,t)}{\int_0^{\infty} C_{\mathrm{app}}(L,t)\mathrm{d}t} = \frac{U}{\sqrt{4\pi at}}\exp\left\{-\frac{(L-Ut)^2}{4at}\right\} \tag{25}$$

Practically, however, the time region may be restricted within the reliable range to avoid experimental error. For example [21,26], $t_1$ and $t_2$ are chosen at 10% of the frontal and the latter peak height of the measured curve, respectively.

The measured and normalized response curves, $\hat{C}_{\mathrm{meas}}(t)$, are compared with the calculated curves, $\hat{C}_{\mathrm{app}}(t)$. The degree of fit can be estimated in terms of the root-mean-square (rms) error defined by Eq. (26):

$$\varepsilon = \left[\frac{\int_{t_1}^{t_2}\{\hat{C}_{\mathrm{meas}}(t) - \hat{C}_{\mathrm{app}}(t)\}^2\mathrm{d}t}{\int_{t_1}^{t_2}\{\hat{C}_{\mathrm{meas}}(t)\}^2\mathrm{d}t}\right]^{1/2} \tag{26}$$

where

$$\hat{C}_{\mathrm{meas}}(t) \equiv \frac{C_{\mathrm{meas}}(t)}{\int_{t_1}^{t_2} C_{\mathrm{meas}}(t)\mathrm{d}t} \tag{26a}$$

Parameter values are determined by minimizing error $\varepsilon$. The unknown parameters of this system are $k$, $D_{12}$ and $u_{\mathrm{a}}$. Because the same values of $U$ and $a$ give the same normalized response curves represented by Eq. (24), $k$ and $D_{12}$ are determined as a function of $u_{\mathrm{a}}$ for a given response curve. Therefore, we have to measure directly the fluid velocity $u_{\mathrm{a}}$ to obtain $k$ and $D_{12}$ for a single pulse injection with a coated column.

Using measured values of $u_{\mathrm{a}}$, the values for $U$ and $a$ are determined by curve fitting. Values for $k$ and $D_{12}$ are obtained by solving Eqs. (7a) and (7d) under condition of Eq. (8) as follows:

$$k = \frac{u_{\mathrm{a}}}{U} - 1 \tag{27}$$

$$D_{12} = \frac{\{(1+6k+11k^2)/(1+k)\}\{(R^2U^2)/(24a)\}}{1+\sqrt{1-[\{(1+6k+11k^2)/(1+k)^2\}\{(R^2U^2)/(12a^2)\}]}} \tag{28}$$

### 3.2. Parameter sensitivity

Parameter sensitivities of $k$ and $D_{12}$ with respect to $u_{\mathrm{a}}$ are given by differentiating $U =$ constant and $a =$ constant as:

$$\frac{u_{\mathrm{a}}}{k}\frac{\mathrm{d}k}{\mathrm{d}u_{\mathrm{a}}} = \frac{1+k}{k} \tag{29}$$

$$\frac{u_{\mathrm{a}}}{D_{12}}\frac{\mathrm{d}D_{12}}{\mathrm{d}u_{\mathrm{a}}} = 1 + \frac{4(1+4k)}{(1+6k+11k^2) - 48(D_{12}/(RU))^2} \cong 1 + \frac{4(1+4k)}{1+6k+11k^2} \tag{30}$$

where the approximation in Eq. (30) is made assuming the validity of Eq. (8). For small $k$, i.e., a weak adsorption system, we obtain $(u_{\mathrm{a}}/k)(\mathrm{d}k/\mathrm{d}u_{\mathrm{a}}) \cong 1/k$ and $(u_{\mathrm{a}}/D_{12})(\mathrm{d}D_{12}/\mathrm{d}u_{\mathrm{a}}) \cong 5$, while for a large $k$, $(u_{\mathrm{a}}/k)(\mathrm{d}k/\mathrm{d}u_{\mathrm{a}}) \cong 1$ and $(u_{\mathrm{a}}/D_{12})(\mathrm{d}D_{12}/\mathrm{d}u_{\mathrm{a}}) \cong 1$. Therefore, for a weak adsorption system, the precise measurement of $u_{\mathrm{a}}$ is needed to estimate $D_{12}$, and the relative error of $D_{12}$ becomes a maximum of five-fold larger than the corresponding error for $u_{\mathrm{a}}$.

### 3.3. Taylor dispersion analysis for weak adsorption

For small $k$, the transport in a coated column in a special case at $k = 0$ may be regarded as the Taylor dispersion. The normalized solution $\hat{C}_{\mathrm{app},0}$ for the Taylor dispersion is obtained by setting $k = 0$ in Eq. (24) as:

$$\hat{C}_{\mathrm{app},0}(t) \equiv \frac{(1/\sqrt{4\pi a_0 t})\exp\{-(L-U_0t)^2/(4a_0t)\}}{\int_{t_1}^{t_2}(1/\sqrt{4\pi a_0 t})\exp\{-(L-U_0t)^2/(4a_0t)\}\mathrm{d}t} \tag{31}$$

where

$$a_0 = D_{12,0} + \frac{R^2{U_0}^2}{48D_{12,0}} \tag{31a}$$

In the Taylor dispersion, two parameter values, $U_0$ and $D_{12,0}$, are obtainable by the curve-fitting method [26]. If Eq. (31) instead of Eq. (24) is used for curve fitting with variable parameters of $U_0$ and $D_{12,0}$, we obtain $U_0 = U$ and $a_0 = a$. Ignoring the first terms in Eqs. (7a) and (31a) gives:

$$D_{12,0} \cong \frac{1+k}{1+6k+11k^2}D_{12} \tag{32}$$

Thus, the relative error is:

$$\frac{D_{12} - D_{12,0}}{D_{12}} \cong \frac{k(5+11k)}{1+6k+11k^2} \tag{33}$$

### 3.4. Moment method

Initial parameter values for the curve-fitting method can be obtained from the first and the second temporal moments of the measured response curve, i.e., mean residence time $\bar{t}$ and variance $\sigma^2$, as:

$$\bar{t} \equiv \frac{\int_0^\infty t C_{\text{meas}}(t)\mathrm{d}t}{\int_0^\infty C_{\text{meas}}(t)\mathrm{d}t} \tag{34}$$

$$\sigma^2 \equiv \frac{\int_0^\infty (t-\bar{t})^2 C_{\text{meas}}(t)\mathrm{d}t}{\int_0^\infty C_{\text{meas}}(t)\mathrm{d}t} \tag{35}$$

Theoretically, from Eq. (12), the first and the second moments at $x = L$ are obtained as:

$$\bar{t} = \frac{\int_0^\infty t C_{\text{app}}(L,t)\mathrm{d}t}{\int_0^\infty C_{\text{app}}(L,t)\mathrm{d}t} = \frac{L}{U}\left(1 + 2\frac{a}{LU}\right) \tag{36}$$

$$\sigma^2 = \frac{\int_0^\infty (t-\bar{t})^2 C_{\text{app}}(L,t)\mathrm{d}t}{\int_0^\infty C_{\text{app}}(L,t)\mathrm{d}t} = 2\left(\frac{L}{U}\right)^2 \frac{a}{LU}\left(1 + 4\frac{a}{LU}\right) \tag{37}$$

While solving Eqs. (36) and (37) for $k$ and $D_{12}$, $k$ is first obtained by:

$$k = \frac{2(2-\alpha)}{3+\sqrt{1+4\alpha}}\frac{u_a \bar{t}}{L} - 1 \tag{38}$$

where

$$\alpha = \frac{\sigma^2}{\bar{t}^2} \tag{38a}$$

Then, $D_{12}$ can be estimated under condition represented by Eq. (8) as:

$$D_{12} \cong \frac{2\gamma}{\beta + \sqrt{\beta^2 - 4\gamma}} L u_a \tag{39}$$

where

$$\beta = \frac{2\alpha - 1 + \sqrt{1+4\alpha}}{4(2-\alpha)} \tag{39a}$$

$$\gamma = \frac{1+6k+11k^2}{(1+k)^2}\frac{R^2}{48L^2} \tag{39b}$$

## 4. Higher-order approximate solution

### 4.1. Modification of Golay equation

The distortion of response curve is related to the third moment. As discussed in Section 2, the first and the second spatial moments of the Gaussian-like approximate solution agree with those for the cylindrical model, but the third moments are different. In fact, $\bar{C}^{(3)}(t)$ does not vanish but $\bar{C}_{\text{app}}{}^{(3)}(t) = 0$. The third moment of the Golay solution does not become zero, implying that the average concentration $C(x, t)$ is expressed more accurately by the Golay solution $C_G(x, t)$ than by the Gaussian-like approximate solution $C_{\text{app}}(x, t)$.

In the Golay model, the overall cross-sectional average concentration is given as $\bar{C}_G(z,t) = (1+k)C_G(z,t)$ by neglecting $\{c(R,z,t) - C_G(z,t)\}$. The first and the second spatial moments of $\bar{C}_G$ agree with those of the Gaussian-like approximate solution, Eqs. (18) and (19). The third moment is given as:

$$\frac{\bar{C}_G{}^{(3)}(t)}{\bar{C}_G{}^{(0)}} = 6abt \tag{40}$$

On the other hand, the third spatial moment for the cylindrical model is given as (Appendix A):

$$\frac{\bar{C}^{(3)}(t)}{\bar{C}^{(0)}} = R^2 U \left\{ \frac{k(1+4k)}{2(1+k)^2} + \frac{1+10k+44k^2+122k^3+177k^4}{(1+k)^2}\frac{R^2U^2}{480{D_{12}}^2} \right\} t + \Xi(t) \tag{41}$$

where $\Xi(t)$ is a function such that $\lim_{t\to\infty}\{\Xi(t)/t\} = 0$.

When the first term is dominant, $b$ in the Golay equation should be changed to $b^*$, the modified Golay equation:

$$b^* = \frac{R^2U}{6a}\left\{ \frac{k(1+4k)}{2(1+k)^2} + \frac{1+10k+44k^2+122k^3+177k^4}{(1+k)^2} \times \frac{R^2U^2}{480{D_{12}}^2} \right\} \tag{42}$$

Under condition of Eq. (8):

$$b^* \cong \frac{1+10k+44k^2+122k^3+177k^4}{(1+k)(1+6k+11k^2)}\frac{R^2U}{60D_{12}} \tag{43}$$

Note that $C_G$ in the modified Golay equation does not reduce to $C_{\text{app}}$ when $k \to 0$. $C_G$ at $k = 0$ is an approximate solution for the Taylor dispersion whose third moment agrees with that for the original model, which is equivalent to the cylindrical model at $k = 0$.

### 4.2. Solution of Golay equation

Under boundary and initial conditions, corresponding to Eqs. (10) and (11) where $C_{\text{app}}$ is replaced by $C_G$, Eq. (7) with $b^*$ is solved (see Appendix B) using:

$$C_G(x,t) = \left(\frac{m}{\pi R^2}\right)\frac{1}{(1+k)b^*}\sqrt{\frac{\tau}{\zeta+\tau}}\exp\{-(\zeta+2\tau)\} \times I_1(2\sqrt{(\zeta+\tau)\tau}) \quad \text{for } x, t > 0 \tag{44}$$

where

$$\zeta = \frac{z}{b^*} = \frac{1}{b^*}(x - Ut) \tag{44a}$$

$$\tau = \frac{a}{b^{*2}}t \tag{44b}$$

and $I_1(w)$ is the modified Bessel function of the first kind of first order, defined as:

$$I_1(w) = \sum_{n=0}^{\infty} \frac{1}{n!(n+1)!}\left(\frac{w}{2}\right)^{2n+1} \quad \text{for } w \geq 0 \tag{44c}$$

Note that when $b^* \to 0$, $C_G$ reduces to $C_{app}$ using the asymptotic properties of the Bessel function, $I_1(w) \to \exp(w)/\sqrt{2\pi w}$ at $w \to \infty$ (for example, see [27]).

The following rms error $\varepsilon_{app}$ is introduced to estimate the difference between $C_G$ and $C_{app}$ at the detecting point ($x = L$):

$$\varepsilon_{app} = \left[\frac{\int_0^\infty \{C_G(L,t) - C_{app}(L,t)\}^2 dt}{\int_0^\infty \{C_G(L,t)\}^2 dt}\right]^{1/2} \tag{45}$$

Error $\varepsilon_{app}$ is characterized by the two parameters, $A$ and $B$:

$$A = \frac{a}{LU} \tag{46}$$

$$B = \frac{b^*}{L} \tag{47}$$

According to practical computation, $\varepsilon_{app}$ can be approximated as:

$$\varepsilon_{app} \approx 0.5\frac{B}{\sqrt{A}} \quad \text{for } A < 0.1 \text{ and } \frac{B}{\sqrt{A}} < 0.08 \tag{48}$$

## 5. Measurements of binary diffusion coefficient and retention factor

### 5.1. Impulse response measurement

The experimental apparatus used for the Taylor dispersion method was described previously [26]. In this study, a diffusion column was replaced by a polymer-coated capillary column (Ultra Alloy CW-15W-1.0F, bonded polyethylene glycol, film thickness = 1 μm, inside diameter = 0.515 mm, length = 15.86 m, coil radius = 135 mm) supplied by Frontier Laboratory, Japan. The radii of both ends of the column were measured with an X-ray micro-analyzer (JEOL, JXA 8900RL, Japan). Total volume of the diffusion column between the injector and detector was evaluated from an impulse response measurement for benzene into a liquid hexane stream at atmospheric pressure and room temperature. Impulse response measurements were conducted by injecting the acetone solution of phenol (0.032 μmol of phenol was loaded in most runs) as a tracer into a supercritical $CO_2$ stream at 313.15 K and 11.6–28.6 MPa. Tracer concentration was measured with a UV-Vis multi-detector (MD-1510, JASCO, Japan) by scanning from 195 to 355 nm at increments of 4 nm. Temporal changes in flow rates were measured with a soap-bubble flowmeter 30–40 times in the course of a single run (from 0 to 80–100 min), and their mean and the ratio of standard deviation to mean were calculated, as shown in Table 1.

Acetone (99.5%, Aldrich) and phenol (99%, Aldrich) were employed without further purification. Wavelengths of 275 and 271 nm were used in the analyses for acetone and phenol, respectively.

### 5.2. Determination of parameter values

As shown in Fig. 2(a) and (b), the measured response curves $\hat{C}_{meas}$, shown as blank circles, for acetone and phenol at 313.15 K and 17.87 MPa are compared to those calculated from Eq. (24) with assumed values of $D_{12}$, and values of $t_1$ and $t_2$ at 10% of the maximum peak height of the measured curve, the same as in measurements of Funazukuri et al. [26]. The degree of fit is estimated by the rms error $\varepsilon$ as defined by Eq. (26). As shown in Fig. 2, we can judge that

Table 1
Fluid velocity $u_{a,meas}$ experimentally measured and the values for binary diffusion coefficient $D_{12}$, retention factor $k$ and fitting error $\varepsilon$ obtained from the curve-fitting method for acetone and phenol in supercritical carbon dioxide at temperature 313.15 K and pressures from 11.6 to 28.6 MPa

| Pressure (MPa) | $u_{a,meas}$ | | Acetone | | | Phenol | | |
|---|---|---|---|---|---|---|---|---|
| | Mean ($10^{-3}$ m s$^{-1}$) | S.D./mean (%) | $D_{12}$ ($10^{-8}$ m$^2$ s$^{-1}$) | $k$ | $\varepsilon$ (%) | $D_{12}$ ($10^{-8}$ m$^2$ s$^{-1}$) | $k$ | $\varepsilon$ (%) |
| 11.64 | 9.434 | 1.16 | 1.843 | 0.0499 | 0.83 | 1.529 | 2.555 | 0.16 |
| 12.61 | 9.347 | 3.61 | 1.768 | 0.0461 | 1.19 | 1.388 | 2.250 | 0.25 |
| 13.54 | 9.097 | 2.83 | 1.731 | 0.0399 | 3.03 | 1.370 | 2.031 | 0.15 |
| 14.37 | 8.804 | 1.74 | 1.675 | 0.0286 | 0.96 | 1.328 | 1.869 | 0.14 |
| 14.43 | 9.076 | 1.53 | 1.664 | 0.0401 | 0.61 | 1.306 | 1.893 | 0.19 |
| 16.13 | 9.144 | 2.01 | 1.592 | 0.0427 | 0.15 | 1.261 | 1.697 | 0.31 |
| 17.37 | 8.765 | 1.36 | 1.540 | 0.0432 | 0.96 | 1.237 | 1.584 | 0.12 |
| 17.87 | 8.840 | 1.03 | 1.505 | 0.0482 | 0.62 | 1.218 | 1.548 | 0.12 |
| 20.11 | 8.697 | 1.46 | 1.443 | 0.0371 | 0.86 | 1.176 | 1.384 | 0.16 |
| 21.90 | 8.641 | 0.81 | 1.387 | 0.0353 | 0.88 | 1.128 | 1.304 | 0.03 |
| 24.68 | 8.499 | 0.92 | 1.338 | 0.0381 | 0.43 | 1.093 | 1.199 | 0.13 |
| 25.09 | 8.620 | 1.05 | 1.337 | 0.0336 | 0.09 | 1.083 | 1.174 | 0.25 |
| 25.30 | 8.254 | 0.85 | 1.349 | 0.0472 | 0.49 | 1.078 | 1.206 | 0.16 |
| 28.58 | 8.365 | 0.78 | 1.267 | 0.0374 | 0.53 | 1.039 | 1.090 | 0.06 |

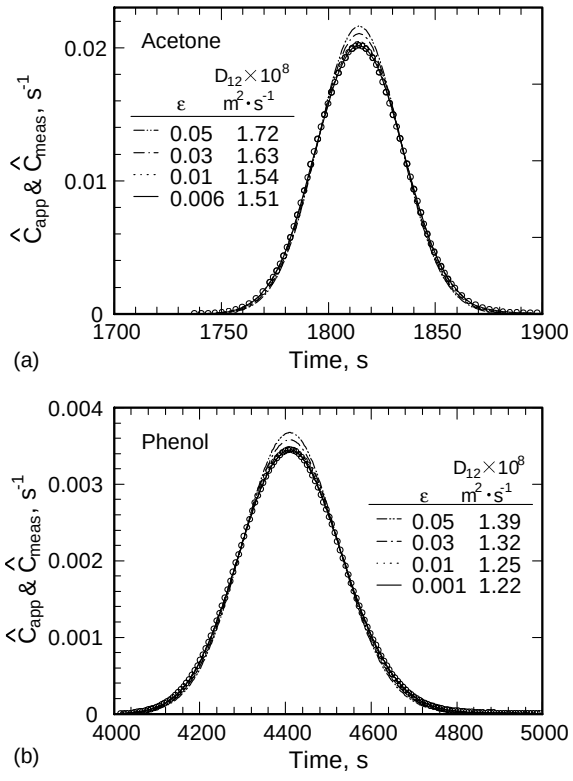


Fig. 2. Comparison of response signal measured (○) at 313.15 K and 17.87 MPa and $u_{a,meas} = 8.84 \times 10^{-3}\,m\,s^{-1}$ with those predicted with some parameter values (lines) for: (a) acetone at 275 nm and $k = 0.0482$; (b) phenol at 271 nm and $k = 1.548$.

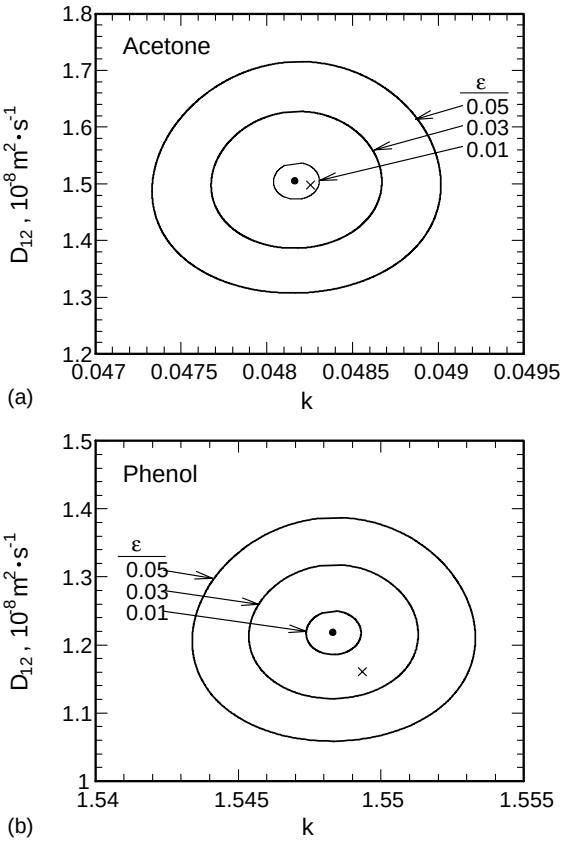


Fig. 3. Error contour map in the plot of $D_{12}$ vs. $k$ for data in Fig. 2 at the measured velocity $u_{a,meas} = 8.84\times10^{-3}\,m\,s^{-1}$ for: (a) acetone; (b) phenol. The dot shows the best-fit point: $k = 0.0482$ and $D_{12} = 1.51\times10^{-8}\,m^2\,s^{-1}$ for acetone and $k = 1.548$ and $D_{12} = 1.22\times10^{-8}\,m^2\,s^{-1}$ for phenol; "×" shows that obtained by the moment method.

the agreement is good for $\varepsilon < 0.01$ and acceptable for $\varepsilon < 0.03$.

Parameter values were determined by minimizing the error. A set of parameter values with the same error value makes a contour in the parameter space. Fig. 3(a) and (b) depict the error contour maps in the $k$–$D_{12}$ plane for the data shown in Fig. 2(a) and (b) at the velocity $u_{a,meas} = 8.84\times10^{-3}\,m\,s^{-1}$. From these figures, $k$ and $D_{12}$ can be estimated simultaneously from a single run as $k = 0.0482$ and $D_{12} = 1.51\times10^{-8}\,m^2\,s^{-1}$ for acetone and $k = 1.548$ and $D_{12} = 1.22\times10^{-8}\,m^2\,s^{-1}$ for phenol. The values obtained by the moment method, calculated from Eqs. (38) and (39), are also shown in Fig. 3 as "×".

The error contours for increasing $u_a$ by 1 and 2% are shown in Fig. 4. The $k$ and $D_{12}$ values minimizing the error are shown in Table 2 for each $u_a$. These figures suggest that it is not possible to determine all three parameters $k$, $D_{12}$, and $u_a$ simultaneously; however, $k$ and $D_{12}$ can be determined when the fluid velocity is given, as discussed in Section 3.1. Parameter sensitivity with respect to $u_a$ also is shown in Table 2. The estimated values in Table 2 agree well with the theoretical values given by Eqs. (29) and (30).

### 5.3. Effects of wavelength

Fig. 5 shows the dependence of wavelength from 195 to 355 nm at increments of 4 nm for the same run in Fig. 2.

Table 2
The best fitted values for the velocity of $u_{a,meas}$, $1.01\times u_{a,meas}$ and $1.02\times u_{a,meas}$ for the response curves in Fig. 2 and their parameter sensitivity to $u_a$

| | $u_a$ ($10^{-3}\,m\,s^{-1}$) | $k$ | $D_{12}$ ($10^{-8}\,m^2\,s^{-1}$) | $\Delta k/k$ (%) | $\Delta D_{12}/D_{12}$ (%) |
|---|---|---|---|---|---|
| Acetone | 8.84 | 0.04816 | 1.505 | – | – |
| | 8.93 | 0.05884 | 1.577 | 22 | 4.8 |
| | 9.02 | 0.06951 | 1.650 | 44 | 9.6 |
| Phenol | 8.84 | 1.5483 | 1.218 | – | – |
| | 8.93 | 1.5743 | 1.240 | 1.7 | 1.8 |
| | 9.02 | 1.6002 | 1.262 | 3.4 | 3.6 |

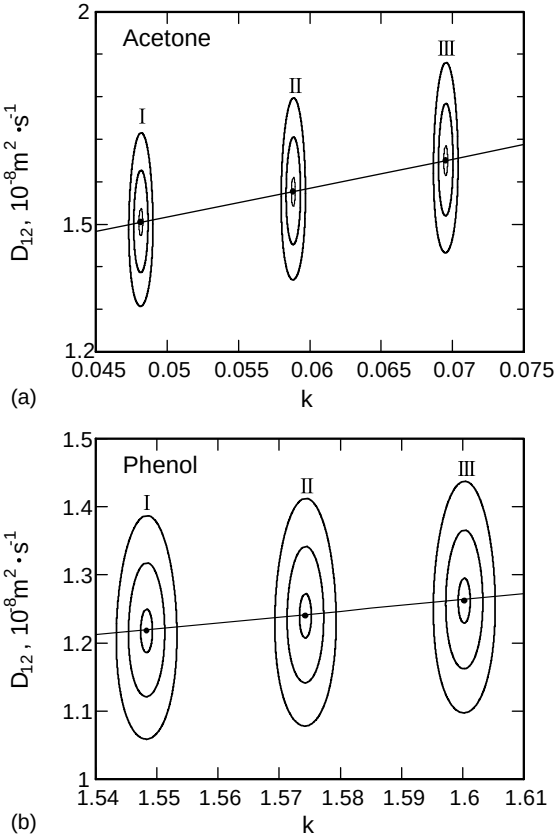


Fig. 4. Error contour map in the plot of $D_{12}$ vs. $k$ for various $u_a$ values at: (I) measured $u_{a,meas}$; (II) $1.01 \times u_{a,meas}$; (III) $1.02 \times u_{a,meas}$ for the data in Fig. 2. Contours show $\varepsilon = 0.05$, 0.03 and 0.01 from the outer side. The best-fit values are listed in Table 2.

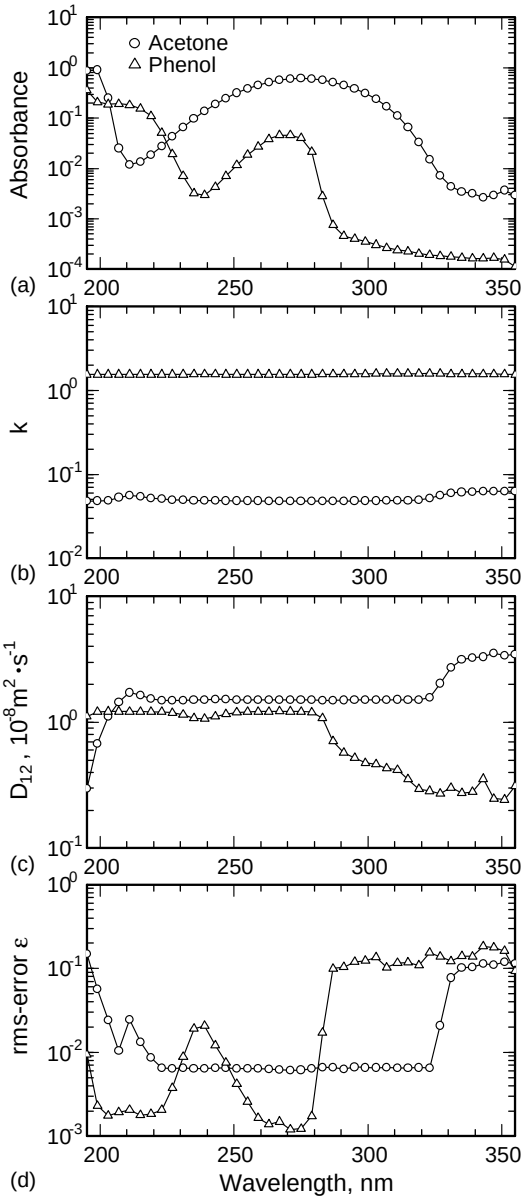


Fig. 5. Effects of wavelength. (a) Absorbance at the peak top of the response curve; $k$ (b), $D_{12}$ (c) and rms error $\varepsilon$ (d) for the same run in Fig. 2 at each wavelength from 195 to 355 nm at increments of 4 nm: (○) acetone; (△) phenol.

In principle, parameter values do not depend on the wavelength, but in reality they do depend on wavelength because of experimental noise or non-linearity of the detector. Strong absorbance is preferable against the noise of the detector signal, but results in a loss of detector linearity. In this study, wavelengths of 275 nm for acetone and 271 nm for phenol were chosen to analyze response curves having moderate absorbance values that resulted in a small fitting error and constant parameter values around these wavelengths, as has been discussed in previous reports [22,26].

### 5.4. Effects of solvent

To examine the influence of solvent on the diffusion of the solute in the column, several pulses of the neat solvent were injected immediately after the pulse of the solution. The solvent pulses passed through the peak of the solute in the column. Fig. 6(a) shows the response curve measured at the column exit when three pulses of acetone were injected. Note that the first peak (#0) of acetone appearing at ca. 1800 s corresponds to the pulse of phenol. Fig. 6(b) and (c) show $k$ and $D_{12}$ values obtained from the response curves passed by several pulses of acetone. Since $k$ and $D_{12}$ do not depend on the number of additional pulses, it can be concluded that the diffusion of phenol in the column is not affected by the solvent.

### 5.5. Effects of secondary flow

Fig. 7 shows the effect of flow rate on the measured $k$ and $D_{12}$ values in terms of $De\,Sc^{1/2}$, where the measured parameters are denoted by $k'$ and $D'_{12}$ and the leveled-off values by $D_{12}$, and $De$ and $Sc$ are the Dean and the Schmidt number, respectively. The flow rates do not affect retention factors, but do $D_{12}$ values, as shown in Fig. 7(a). The error in $D_{12}$ ascribed to secondary flow due to column coiling

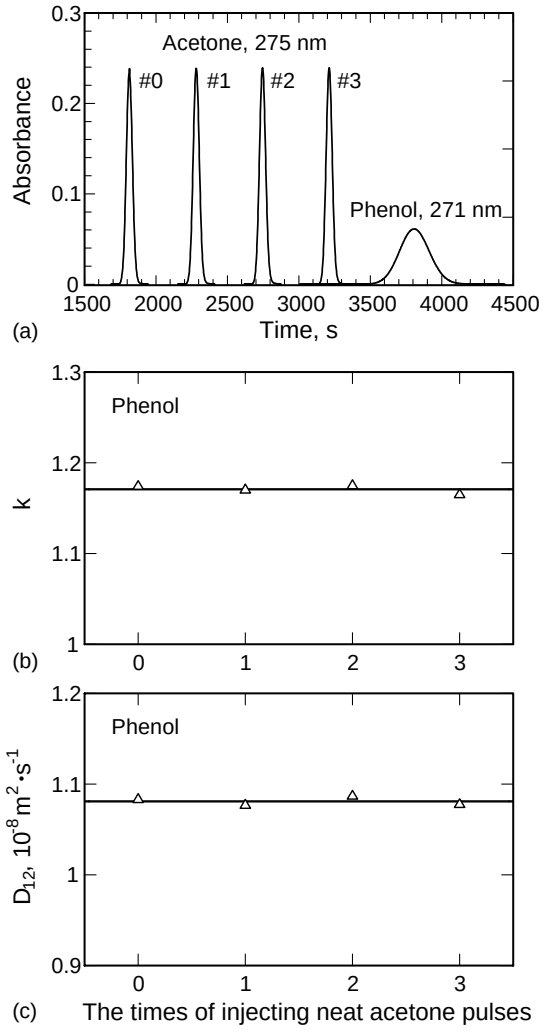


Fig. 6. Effects of solvent. (a) Response curves (chromatograms) for three acetone pulses after loading a pulse of phenol in acetone, measured at 313.15 K, and 25.09 MPa; $k$ (b) and $D_{12}$ (c) for phenol vs. the injection times of the acetone pulses, where zero in the $x$-axis designates the injection of phenol dissolved in acetone.

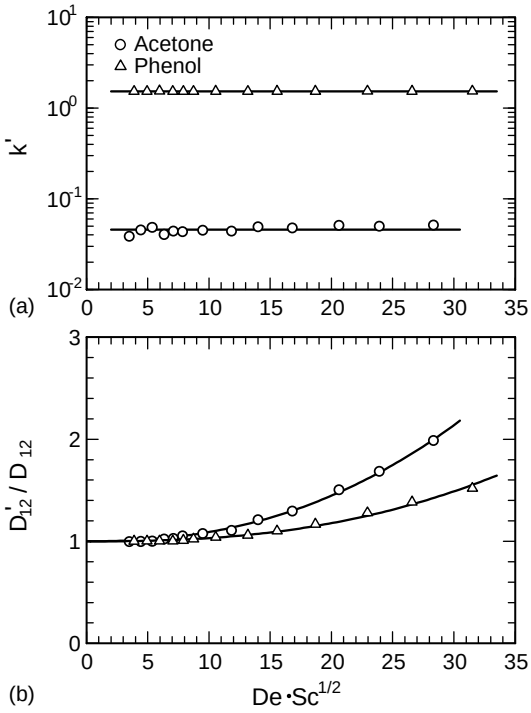


Fig. 7. Effects of the secondary flow on apparent $k'$ (a) and the ratio of apparent $D_{12}'$ to the leveled-off $D_{12}$ value (b), measured at 313.15 K and 17.87 MPa: (○) acetone; (△) phenol.

is less than 1% [25] by the criterion $De\,Sc^{1/2} < 8$ with an uncoated capillary column. But the effect was not clarified with a coated column. Recently, the authors [28] report that the retention factor is not influenced by secondary flow and the effect on the binary diffusion coefficient with a coated capillary column becomes small for large retention factors. In fact, as shown in Fig. 7(b), $D_{12}$ for phenol is less influenced by secondary flow than that for acetone. Although the criterion can be relaxed with a coated capillary column, the flow rate for the measurement was restricted to $De\,Sc^{1/2} < 8$ in this study.

### 5.6. Infinite dilution for binary diffusion coefficients

Fig. 8 plots the effect of different phenol column-loading amounts on determined values and rms error. Since absorbance of the response curve decreases in proportional to the amount of phenol, a smooth response curve cannot be obtained at extremely low injected amount. When a noise elimination procedure is used, a signal can be extracted by removing high frequency noises from an observed signal [29]. As shown in this figure, for injected amounts from 0.0003 to 0.06 μmol, $D_{12}$ values are nearly constant, and no dependence of solute concentration on the $D_{12}$ values is observed. When amounts of phenol injected are lower than $10^{-3}$ μmol, fitting errors are larger because the noise signals are competitive with the original signal. After noise elimination treatment, however, the $D_{12}$ data become consistent with the value for injected amounts from 0.0003 to 0.06 μmol. Thus, the $D_{12}$ values obtained for injected phenol amounts lower than $10^{-1}$ μmol can be considered at infinite dilution. The $D_{12}$ data for phenol in present and previous studies [21] were measured in this range. Note that maximum phenol concentration at the detector among the data plotted in Fig. 8 (4.9 μmol) is $3.1 \times 10^{-4}$ in mole fraction, much lower than the solubility of 0.021 in mole fraction as estimated in the literature at 309 and 333 K by Van Leer and Paulaitis [30] and at 333 to 363 K by García-González et al. [31].

### 5.7. Correlation of binary diffusion coefficients

As described in previous studies under supercritical conditions [21], the retention factor is correlated well with fluid density, and the binary diffusion coefficient with viscosity well. Fig. 9 shows the correlations of: (a) $k$ with $CO_2$ density; and (b) $D_{12}$ with $CO_2$ viscosity. The solid lines show the

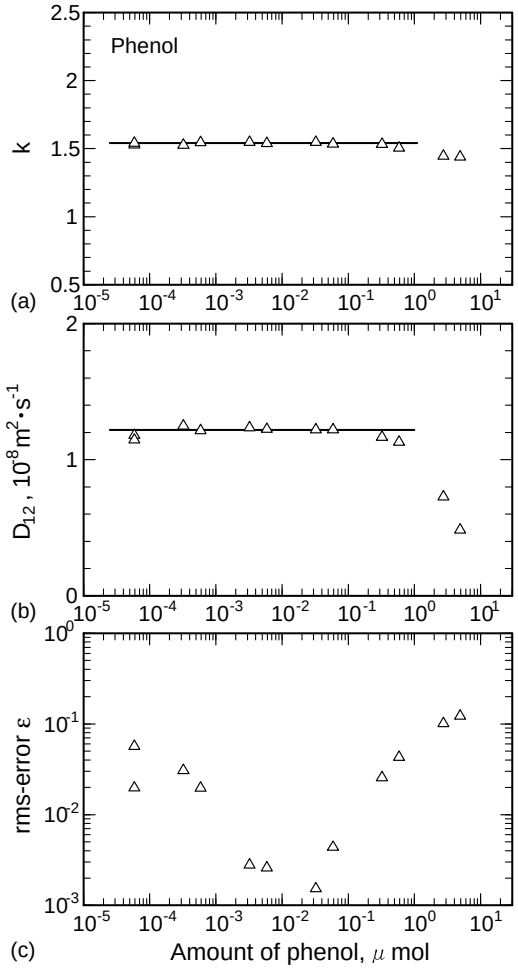


Fig. 8. Effects of the injected solute amount on $k$ (a), $D_{12}$ (b), and rms error $\varepsilon$ (c) for phenol, measured at 313.15 K and 17.87 MPa.

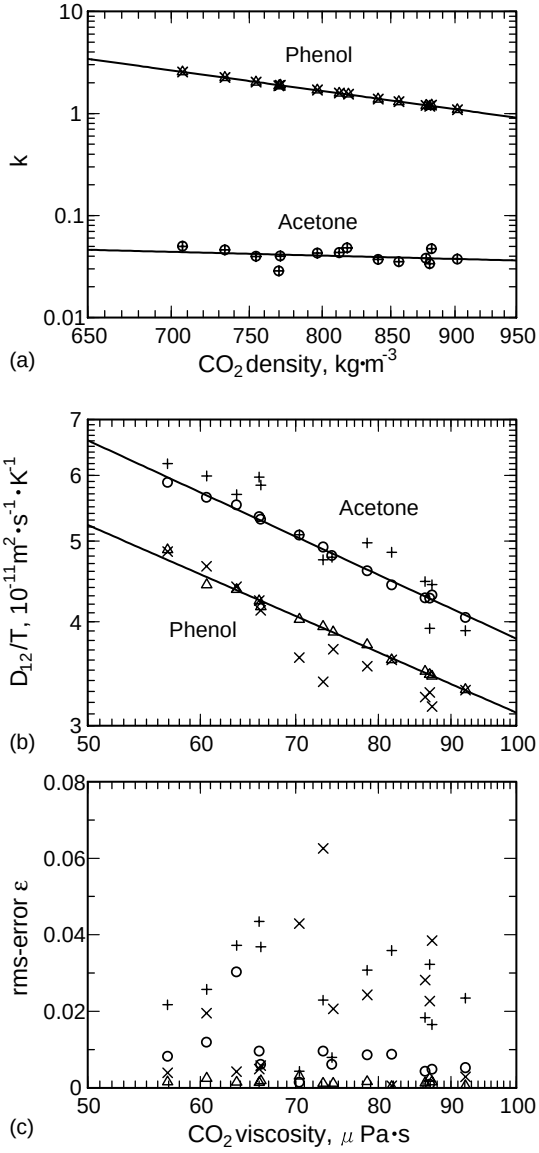


Fig. 9. Comparison of the parameter values and fitting errors for the curve-fitting and moment methods for acetone and phenol at 313.15 K. (a) $k$ vs. $CO_2$ density; $D_{12}/T$ (b) and rms error (c) $\varepsilon$ vs. $CO_2$ viscosity: (○, △) curve-fitting method for acetone and phenol, and (+, ×) moment method for acetone and phenol, respectively.

correlation for data obtained with the curve-fitting method. Fig. 9(c) plots the fitting error. The values by the moment method are also shown in these figures by "+" and "×" for acetone and phenol, respectively. As noted (refer to [19]), the values obtained by the moment method are influenced directly by experimental errors in the frontal and tailing portions of the response curve, especially for higher moments. In fact, the retention factors obtained from the first moment agree well with those obtained by the curve-fitting method. However, the binary diffusion coefficients from the second moment deviate from those obtained by the curve-fitting method.

In Fig. 10(a), $D_{12}$ values for acetone are compared with those obtained from the Taylor dispersion method [26,32]. $D_{12}$ values for phenol are compared in Fig. 10(b) with those obtained from the input–output response technique with an uncoated capillary column connected after a coated column, the so-called the modified Taylor dispersion method [33]. Solid lines indicate the correlations of the present data, which agree well. This evidence validates the use of a polymer-coated capillary column for measurements of binary diffusion coefficients under supercritical conditions.

## 6. Discussion

### 6.1. Effect of surface diffusion

The effect on determined parameter values of the adsorbed species diffusing on the surface of a polymer film coated on the column wall due to the concentration gradient is examined. In this case, Eq. (4) is modified to contain the

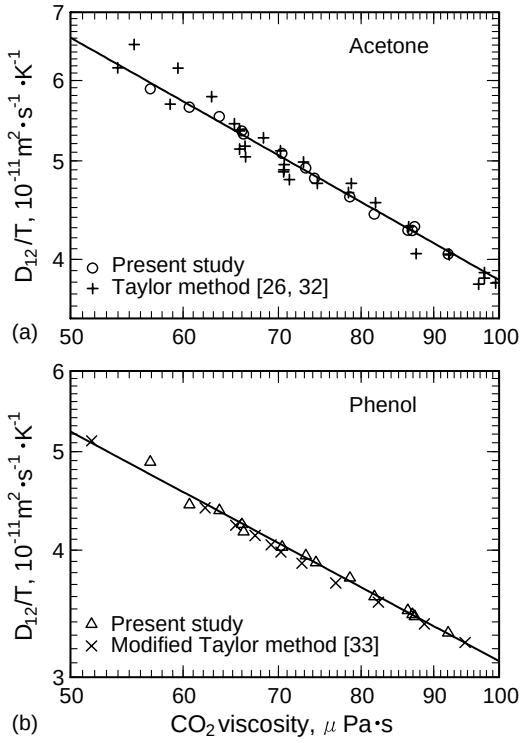


Fig. 10. $D_{12}/T$ vs. $CO_2$ viscosity for (a) acetone and (b) phenol, together with literature data obtained using the original [26,32] and modified [33] Taylor dispersion methods: (○, △) present data for acetone and phenol, and (+, ×) literature data for acetone [26,32] and phenol [33], respectively.

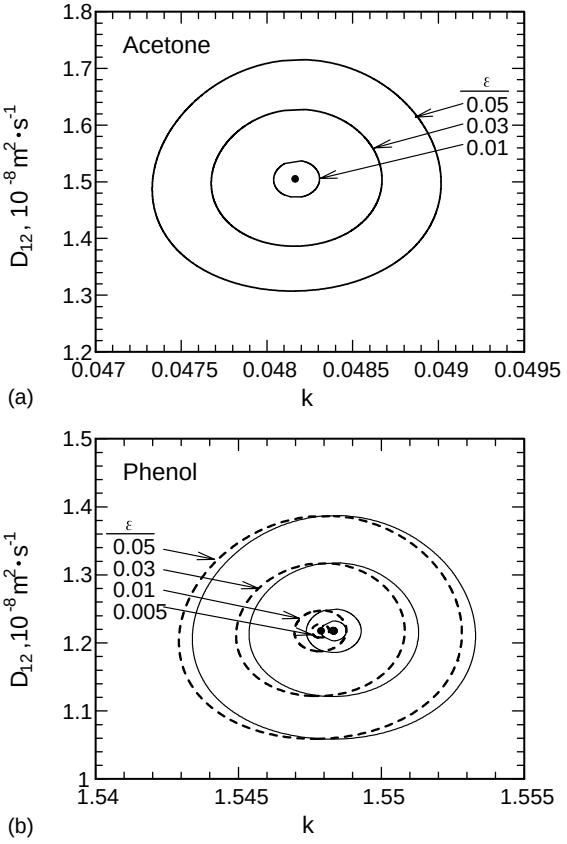


Fig. 11. Error contour map for the plot of $D_{12}$ vs. $k$ for acetone (a) and phenol (b), based on the modified Golay solution for the same run shown in Fig. 2: (—) Gaussian-like approximate solution; (– – –) modified Golay solution.

term of surface diffusion as:

$$k\frac{\partial c}{\partial t} = kD_s\frac{\partial^2 c}{\partial x^2} - \frac{2D_{12}}{R}\frac{\partial c}{\partial r} \quad \text{at } r = R \tag{49}$$

where $D_s$ is the surface diffusion coefficient based on the adsorbate concentration gradient.

This modification does not influence the zeroth and first moments, but does influence the second moment. In fact, $a$ in Eq. (16) should be replaced by $a^*$ as:

$$a^* = \frac{D_{12} + kD_s}{1+k} + \frac{1+6k+11k^2}{1+k}\frac{R^2U^2}{48D_{12}} \tag{50}$$

Since $D_s$ is expected to be lower than $D_{12}$ and the second term is dominant in Eq. (50), the surface diffusion does not need to be considered in impulse response measurements with a coated column.

### 6.2. Validity of the approximation

The accuracy of the Gaussian-like approximate solution is estimated by $\Gamma(t)$ in Eq. (16). In the measurement for acetone in Fig. 2(a), $\Gamma(t)/(2at) \cong 0.0002$–$0.0004$ for the range of $t = 1700$–$1900$ s, and for phenol in Fig. 2(b), $\Gamma(t)/(2at) \cong 0.0001$–$0.0003$ for $t = 4000$–$5000$ s. The second term in $\Gamma(t)$ of Eq. (16a) is negligible for acetone and phenol. According to Eq. (23), the difference in the diffusion coefficients is smaller than 0.04%, which is smaller than the accuracy of the parameter as shown in Fig. 3. Of course, agreement in the first and the second moments does not always result in identical response curves. Although the response curve shows a distortion, which is characterized by the third moment, the Gaussian-like approximate solution does not express the distortion sufficiently.

Fig. 11 compares the error contour maps between the modified Golay solution and Gaussian-like approximate solution. Since the error contours for both models coincide as shown in Fig. 11(a), no difference exists between the two solutions for acetone. However, for phenol in Fig. 11(b), $k$ depends on the model only slightly, but $D_{12}$ does not depend on the model at all. While the contour appears to shift horizontally slightly, the values for $k$ and $D_{12}$ were consistent in both models (difference of best-fitted $k$ values was 0.03%). Analysis of the spatial moment revealed that the third moment of the cylindrical model is positive. However, tailing results in negative values for the third moment. Therefore, tailing of the response curves cannot be explained by this model. As noted by Madras et al. [24], another model must be introduced to describe the tailing.

The difference between $C_{app}$ and $C_G$ is less than 0.6%, according to Eq. (48). In our case, the Gaussian-like approximate solution well predicted response curves measured. Consequently, $C$ is approximated by $C_{app}$ with good

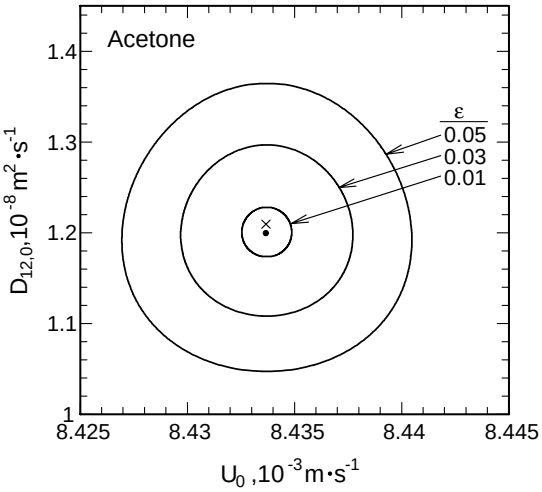


Fig. 12. Error contour map in the plot of $D_{12,0}$ vs. $U_0$ for acetone shown in Fig. 2(a) at 313.15 K and 17.87 MPa: (·) best-fit point; (×) obtained by the moment method.

accuracy. It should be noted that the moment method cannot assure validity of the models because agreement of the first and the second moments in the models do not certify that of response curves predicted by models and measured experimentally.

### 6.3. Estimation of diffusion coefficient for weak adsorption

Since $k$ is very small for acetone, the transport of acetone in a coated column, assuming $k = 0$ as shown in Eq. (31), may be equivalent to the Taylor dispersion. For acetone in Fig. 2(a), the error contour map in the $U_0$–$D_{12,0}$ plane is obtained as shown in Fig. 12. According to this error contour map, $U_0 = 8.434 \times 10^{-3}\,\mathrm{m\,s^{-1}}$ and $D_{12,0} = 1.20 \times 10^{-8}\,\mathrm{m^2\,s^{-1}}$ can be determined simultaneously. For the measurements here, accuracy of $u_a$ was estimated as ±1% (Table 1). From Eq. (30), the relative error of $D_{12}$ is estimated as ±4.6% when adsorption is considered (assuming $k \neq 0$). In contrast, when adsorption of acetone is ignored (assuming $k = 0$), the error becomes 20% according to Eq. (33).

Adsorption of tracer components on the uncoated column wall occurs especially in the near-critical region, even for weak polar compounds such as naphthalene [15]. Despite the weak adsorption, it cannot be ignored for the determination of diffusion coefficients when the value of the relative error of Eq. (33) is not negligible. In the Taylor dispersion by both the curve-fitting and the moment method, the measurement of solvent flow velocity $u_a$ is not required for determining $D_{12}$ values. However, the impulse response method with a polymer-coated column by the curve-fitting method requires the determination of $u_a$ as accurately as possible to determine $k$ and $D_{12}$ because the sensitivity for $D_{12}$ is nearly five-fold larger than that for $u_a$ when $k$ is small. Although a more experimental burden in the $u_a$ measurement is needed with a polymer-coated column, the effect of solute adsorption on the inner wall of the column on $D_{12}$ value can be reduced significantly. Therefore, diffusion coefficient measurements with a coated capillary column possess an advantage over those by the Taylor dispersion when determining diffusion coefficients, unless adsorption is negligible.

### 6.4. Effect of determination error of column radius

The accurate radius and length of the diffusion column are essential in the determination of binary diffusion coefficients. However, column radius may be difficult to measure. In this section, the effect of determination error of column radius on the parameter values is examined.

For a single run, $U$ and $a$ can be obtained from the curve-fit, and the flow rate, $\pi R^2 u_a$, is measured. By differentiating $U$ = constant, $a$ = constant and $R^2 u_a$ = constant, the sensitivities to $R$ are:

$$\frac{R}{k}\frac{\mathrm{d}k}{\mathrm{d}R} = -\frac{2(1+k)}{k} \tag{51}$$

$$\frac{R}{D_{12}}\frac{\mathrm{d}D_{12}}{\mathrm{d}R} \cong -\frac{8(1+4k)}{1+6k+11k^2} \tag{52}$$

where Eq. (52) is derived with Eq. (8). When $k$ is small, the $D_{12}$ error is almost eight times as large as that of $R$. As $k$ becomes larger, however, the $D_{12}$ error decreases. The column radius should be measured as accurately as possible for measurements with small $k$ values.

In the Taylor dispersion method, $U_0$ and $a_0$ are given from the measurement. Then,

$$\frac{R}{D_{12}}\frac{\mathrm{d}D_{12}}{\mathrm{d}R} \cong 2 \tag{53}$$

Thus, the $D_{12}$ error is twice as large as that of $R$. Consequently, the more accurate measurement of $R$ is required in the chromatographic impulse response method than in the Taylor method. In contrast, when $k$ is large, the relative $D_{12}$ error is small. This results in the advantage of the chromatographic impulse response method over the Taylor dispersion method. For instance, when $k > 1.2$, $(\Delta D_{12}/D_{12}) < 2(\Delta R/R)$.

### 6.5. Measurements in the near-critical region

Recently, critical anomalies in diffusion coefficients measured by the Taylor dispersion method have been reported [34–36]. However, Levelt Sengers et al. [37] reported difficulty in obtaining measurements in the near-critical region by the Taylor dispersion method.

As mentioned earlier, adsorption of a solute on a column wall may occur in the near-critical region [15]. This effect is reduced in the chromatographic impulse response method as compared with the Taylor dispersion method. When the velocity of a supercritical fluid has a parabolic profile, measurements obtained by the chromatographic impulse response method are reliable even in the near-critical region. However, the measurements are based on assumptions such as

a constant supercritical fluid velocity and independence of the diffusion coefficient and retention factor from concentration. These assumptions, which are true far from the critical points, have not been verified in the near-critical region because large negative values of partial molar volumes for solutes have been reported. Since the barycentric motion significantly affects the mass transfer in the critical region, as noted by Clifford and Coleby [38], the further studies are needed for measurements in flowing systems such as in the chromatographic impulse response method as well as the Taylor dispersion method.

### 6.6. Boundary condition used by Lai and Tan

Lai and Tan [18] employed the following condition instead of Eq. (11):

$$C'_{\mathrm{app}} = \left(\frac{m}{\pi R^2}\right)\frac{\delta(t)}{u_{\mathrm{a}}} \quad \text{at } x = 0 \tag{54}$$

The Gaussian-like approximate solution is obtained from Eqs. (9), (10), and (54) as:

$$C'_{\mathrm{app}}(x,t) = \left(\frac{m}{\pi R^2}\right)\frac{x}{u_{\mathrm{a}}t}\frac{1}{\sqrt{4\pi a t}}\exp\left\{-\frac{(x-Ut)^2}{4at}\right\} \quad \text{for } x, t > 0 \tag{55}$$

and the temporal moments at $x = L$ are expressed as:

$$\bar{t}' = \frac{L}{U} \tag{56}$$

$$\sigma'^2 = 2\left(\frac{L}{U}\right)^2\frac{a}{LU} \tag{57}$$

The value of $a/(LU)$ is much smaller than unity under their experimental conditions as well as under the present conditions; for example, $a/(LU) = 6 \times 10^{-5}$ in case of Fig. 2(a). Although Eq. (54) does not appear to represent the experimental conditions, the difference in measured $k$ and $D_{12}$ values caused by differences in initial conditions between Eqs. (11) and (54) is negligible under these experimental conditions.

## 7. Conclusions

The Gaussian-like approximate solution based on a linear and equilibrium adsorption isotherm was shown effective and accurate for determining binary diffusion coefficients and retention factors for highly viscous liquids or solids in supercritical fluids from response curves obtained by the chromatographic impulse response technique with a polymer-coated capillary column using curve fitting. The sensitivities of $D_{12}$ and $k$ to average fluid velocity $u_{\mathrm{a}}$ was derived from the Gaussian-like approximate solutions. Moreover, the Golay equation was modified to allow agreement of the third moment with that of the cylindrical model. The tailing of the response curves cannot be explained by linear and equilibrium adsorption from the third moment.

The applicability of the Gaussian-like approximate solution was experimentally demonstrated with a poly(ethylene glycol)-coated capillary column using phenol dissolved in acetone injected into a laminar flow of supercritical carbon dioxide at 313.15 K and 11.6–28.6 MPa. By comparing measured and calculated response curves for both phenol and acetone individually, infinite-dilution binary diffusion coefficients and retention factors for both compounds were determined simultaneously for each injection when fluid velocity was measured experimentally. The binary diffusion coefficients determined for acetone and phenol agreed with those for each compound separately as reported in the literature.

Reliability of the parameter values was examined by error-map analysis of the response curves. Potential errors were evaluated by considering the compatibility of the measured curves with the predicted ones. The effects of wavelength and secondary flow on the determined values are discussed. The system was at an infinite dilution, which was confirmed by injecting solutions at different concentrations over a wide range of solute quantities. To examine the effect of an organic solvent (acetone) on the determined binary diffusion coefficients, several pulses of acetone were injected to the diffusion column immediately after the injection of phenol dissolved in acetone. Whereas the acetone pulses passed the phenol peak, the solvent (acetone) did not affect the determined binary diffusion coefficients for phenol.

Concerning error ascribed to uncertainty in diffusion column diameter, the more accurate measurement is required in the chromatographic impulse response method than in the Taylor dispersion method when $k$ is small, i.e., for low and non-polar compounds. In contrast, when $k$ is large, i.e., for polar and/or large molecular compounds, the chromatographic impulse response method is more suitable than the Taylor dispersion method because the relative $D_{12}$ error is smaller.

## 8. Nomenclature

| | |
|---|---|
| $a$, $a_0$, $a^*$ | defined by Eqs. (7a), (31a) and (50), respectively ($\mathrm{m^2\,s^{-1}}$) |
| $A$ | defined by Eq. (46) |
| $b$, $b^*$ | defined by Eqs. (7b) and (42), respectively (m) |
| $B$ | defined by Eq. (47) |
| $c(r, x, t)$ | tracer concentration in cylindrical column ($\mathrm{mol\,m^{-3}}$) |
| $C(x, t)$ | cross-sectional average concentration, defined by Eq. (6) ($\mathrm{mol\,m^{-3}}$) |
| $C_{\mathrm{app}}(x, t)$ | Gaussian-like approximate solution, given by Eq. (12) ($\mathrm{mol\,m^{-3}}$) |
| $\hat{C}_{\mathrm{app}}(t)$ | normalized concentration at $x = L$, defined by Eq. (24) ($\mathrm{s^{-1}}$) |

| | |
|---|---|
| $\hat{C}_{\mathrm{app},0}(t)$ | normalized concentration at $x = L$ based on the Taylor dispersion, defined by Eq. (31) ($s^{-1}$) |
| $C_{\mathrm{G}}(x, t)$ | cross-sectional average concentration given by the Golay equation (Eq. (7)) ($mol\,m^{-3}$) |
| $C_{\mathrm{meas}}(t)$ | impulse response curve experimentally measured at $x = L$ ($mol\,m^{-3}$) |
| $\hat{C}_{\mathrm{meas}}(t)$ | normalized impulse response curve experimentally measured at $x = L$, defined by Eq. (26a) ($s^{-1}$) |
| $D_{12}$ | binary diffusion coefficient ($m^2\,s^{-1}$) |
| $D'_{12}$ | apparent binary diffusion coefficient including secondary flow effect ($m^2\,s^{-1}$) |
| $D_{12,0}$ | binary diffusion coefficient based on the Taylor dispersion ($m^2\,s^{-1}$) |
| $D_{\mathrm{s}}$ | surface diffusion coefficient ($m^2\,s^{-1}$) |
| $De$ | Dean number ($=(2Ru_{\mathrm{a}}\rho/\eta)\sqrt{R/R_{\mathrm{coil}}}$) |
| $I_0(x)$, $I_1(x)$ | modified Bessel functions of the first kind of zeroth and first order, defined by Eqs. (B.9a) and (44c), respectively |
| $J_0(x)$, $J_1(x)$ | Bessel functions of the first kind of zeroth and first order, respectively |
| $k$ | retention factor for polymer layer to supercritical fluid |
| $k'$ | apparent retention factor including secondary flow effect |
| $L$ | distance between the injection and detecting points (m) |
| $m$ | total amount of tracer input (mol) |
| $r$ | radial distance variable (m) |
| $R$ | column radius (m) |
| $R_{\mathrm{coil}}$ | coil radius (m) |
| $Sc$ | Schmidt number ($=\eta/(\rho D_{12})$) |
| $t$ | time (s) |
| $\bar{t}$ | mean residence time, defined by Eq. (34) (s) |
| $u_{\mathrm{a}}$ | average fluid velocity ($m\,s^{-1}$) |
| $U$ | $=u_{\mathrm{a}}/(1+k)$ ($m\,s^{-1}$) |
| $U_0$ | fluid velocity based on the Taylor dispersion ($m\,s^{-1}$) |
| $x$ | axial distance variable (m) |
| $z$ | axial distance variable on the moving coordinate, defined by Eq. (7c) (m) |

*Greek letters*

| | |
|---|---|
| $\Gamma(t)$ | the residual part of the second moment, defined in Eq. (16) ($m^2$) |
| $\delta(t)$, $\delta(x)$ | Dirac's delta functions ($s^{-1}$ and $m^{-1}$, respectively) |
| $\varepsilon$, $\varepsilon_{\mathrm{app}}$ | rms error defined by Eqs. (26) and (45), respectively |
| $\eta$ | viscosity (Pa s) |
| $\Lambda(t)$ | defined in Eq. (20) |
| $\lambda_n$ | $n$th positive root of Eq. (16b) |
| $\Xi(t)$ | defined in Eq. (41) ($m^3$) |
| $\rho$ | density ($kg\,m^{-3}$) |
| $\sigma^2$ | second-order temporal moment, defined by Eq. (35) ($s^2$) |
| $\phi$ | angular variable |

*Superscripts*

| | |
|---|---|
| $(n)$ | $n$th order spatial moment with respect to $z$ |
| – | overall cross-sectional average, defined as total quantity of solute both in fluid and in polymer phase per cross-sectional area |

**Acknowledgements**

The authors are grateful to the Ministry of Education, Culture, Sports, Science and Technology for a grant-in-aid (nos. 13650817 and 14655284). The authors also thank Mr. Yasuaki Shimada at the Instrumental Analysis Center, Yokohama National University, for measuring the inner column diameters with an X-ray micro-analyzer.

## Appendix A. Spatial moments for capillary column

The angular variable $\phi$ is eliminated for convenience in this appendix. Transferring the space variable $z$ from $x$, Eqs. (1)–(5) are written as:

$$\frac{\partial c}{\partial t} = D_{12}\left\{\frac{1}{r}\frac{\partial}{\partial r}\left(r\frac{\partial c}{\partial r}\right) + \frac{\partial^2 c}{\partial z^2}\right\} - u(r)\frac{\partial c}{\partial z} + U\frac{\partial c}{\partial z} \tag{A.1}$$

$$k\left(\frac{\partial c}{\partial t} - U\frac{\partial c}{\partial z}\right) = -\frac{2D_{12}}{R}\frac{\partial c}{\partial r} \quad \text{at } r = R \tag{A.2}$$

$$\frac{\partial c}{\partial r} = \text{finite} \quad \text{at } r = 0 \tag{A.3}$$

$$c = 0 \quad \text{at } z = \pm\infty \tag{A.4}$$

$$c = \left(\frac{m}{\pi R^2}\right)\frac{\delta(z)}{1+k} \quad \text{at } t = 0 \tag{A.5}$$

where

$$u(r) = 2u_{\mathrm{a}}\left\{1 - \left(\frac{r}{R}\right)^2\right\} \tag{A.5a}$$

Using the $n$th spatial moment $c^{(n)}(r, t)$ defined by Eq. (13), Eqs. (A.1)–(A.5) become:

$$\frac{\partial c^{(n)}}{\partial t} = D_{12}\frac{1}{r}\frac{\partial}{\partial r}\left(r\frac{\partial c^{(n)}}{\partial r}\right) + n(n-1)D_{12}c^{(n-2)} + nu(r)c^{(n-1)} - nUc^{(n-1)} \tag{A.6}$$

$$k\left(\frac{\partial c^{(n)}}{\partial t} + nUc^{(n-1)}\right) = -\frac{2D_{12}}{R}\frac{\partial c^{(n)}}{\partial r} \quad \text{at } r = R \tag{A.7}$$

$$\frac{\partial c^{(n)}}{\partial r} = \text{finite} \quad \text{at } r = 0 \tag{A.8}$$

$$\left.\begin{aligned} c^{(0)} &= \frac{1}{1+k}\left(\frac{m}{\pi R^2}\right) \\ c^{(n)} &= 0 \quad \text{for } n \neq 0 \end{aligned}\right\} \quad \text{at } t = 0 \tag{A.9}$$

The cross-sectional average of $c^{(n)}(r, t)$ is defined by:

$$C^{(n)}(t) = \frac{2}{R^2}\int_0^R c^{(n)}(r, t) r \, \mathrm{d}r \tag{A.10}$$

And the overall cross-sectional average $\bar{C}^{(n)}(t)$ is defined as the average of the total quantities both dissolved in the fluid and absorbed on the wall:

$$\bar{C}^{(n)}(t) = C^{(n)}(t) + kc^{(n)}(R, t) \tag{A.11}$$

From Eqs. (A.6)–(A.9), the equations for $\bar{C}^{(n)}(t)$ can be derived as:

$$\frac{\mathrm{d}\bar{C}^{(n)}}{\mathrm{d}t} = -nU\bar{C}^{(n-1)} + n(n-1)D_{12}C^{(n-2)} + n\frac{2}{R^2}\int_0^R u(r)c^{(n-1)}(r, t) r \, \mathrm{d}r \tag{A.12}$$

$$\left.\begin{aligned} \bar{C}^{(0)} &= \frac{m}{\pi R^2} \\ \bar{C}^{(n)} &= 0 \quad \text{for } n \neq 0 \end{aligned}\right\} \quad \text{at } t = 0 \tag{A.13}$$

For the zeroth moment, Eqs. (A.12) and (A.13) with $n = 0$ give:

$$\bar{C}^{(0)}(t) = \frac{m}{\pi R^2} \tag{A.14}$$

and Eqs. (A.6)–(A.9) can also be solved

$$c^{(0)}(r, t) = C^{(0)}(t) = \frac{1}{1+k}\left(\frac{m}{\pi R^2}\right) \tag{A.15}$$

For the first moment, Eqs. (A.12) and (A.13) give:

$$\bar{C}^{(1)}(t) = 0 \tag{A.16}$$

and Eqs. (A.6)–(A.9) with $n = 1$ are solved as:

$$c^{(1)}(r, t) = \frac{R^2 u_a c^{(0)}}{4D_{12}}\left[\left\{\frac{1}{2}\left(\frac{r}{R}\right)^4 - \frac{1+2k}{1+k}\left(\frac{r}{R}\right)^2 + \frac{2+8k+9k^2}{6(1+k)^2}\right\} - \sum_{n=1}^{\infty} A_n J_0\left(\lambda_n \frac{r}{R}\right) \times \exp\left(-\lambda_n^2 \frac{D_{12}t}{R^2}\right)\right] \tag{A.17}$$

where $\lambda_n$ is the $n$th positive root of Eq. (16b) and $A_n$ is determined as:

$$\sum_{n=1}^{\infty} A_n J_0\left(\lambda_n \frac{r}{R}\right) = \frac{1}{2}\left(\frac{r}{R}\right)^4 - \frac{1+2k}{1+k}\left(\frac{r}{R}\right)^2 + \frac{2+8k+9k^2}{6(1+k)^2} \tag{A.18}$$

Cross-sectional average of $c^{(1)}(r, t)$ is calculated from Eq. (A.17) as:

$$C^{(1)}(t) = \frac{R^2 u_a c^{(0)}}{4D_{12}}\left[\frac{k(1+4k)}{6(1+k)^2} + k\sum_{n=1}^{\infty} A_n J_0(\lambda_n) \times \exp\left(-\lambda_n^2 \frac{D_{12}t}{R^2}\right)\right] \tag{A.19}$$

Since $C^{(1)} = 0$ at $t = 0$, we obtain:

$$\sum_{n=1}^{\infty} A_n J_0(\lambda_n) = -\frac{1+4k}{6(1+k)^2} \tag{A.20}$$

In order to obtain $A_n$, integrate Eq. (A.18) multiplied by $\{J_0(\lambda_m r/R)(r/R)\}$ in the range of $r = 0$–$R$:

$$\left(1 + \frac{k^2}{4}\lambda_m^2\right) A_m J_0(\lambda_m) - k\sum_{n\neq m} A_n J_0(\lambda_n) = -\frac{32(1+k)}{\lambda_m^4} + \frac{k(1+4k)}{6(1+k)^2} \tag{A.21}$$

Considering Eq. (A.20), $A_m$ is given as:

$$A_m = -\frac{32}{\lambda_m^4 J_0(\lambda_m)} \frac{1}{1 + (k^2/(4(1+k)))\lambda_m^2} \tag{A.22}$$

For the second moment, from Eq. (A.17):

$$\frac{2}{R^2}\int_0^R u(r)c^{(1)}(r, t) r \, \mathrm{d}r = \frac{R^2 {u_a}^2 c_0}{2D_{12}}\left[\frac{1+6k+11k^2}{24(1+k)^2} + 4(1+k)\sum_{n=1}^{\infty}\frac{A_n J_0(\lambda_n)}{\lambda_n^2} \times \exp\left(-\lambda_n^2 \frac{D_{12}t}{R^2}\right)\right] \tag{A.23}$$

In case of $n = 2$, integrating Eq. (A.12) with A.13, Eq. (16) can be obtained.

From Eqs. (A.6)–(A.9), $c^{(2)}(r, t)$ can be expressed as:

$$c^{(2)}(r, t) = 2ac^{(0)}t + g_2(r) + h_2(r, t) \tag{A.24}$$

where

$$g_2(r) = \frac{R^2 c^{(0)}}{4}\left[\frac{k}{1+k}\left\{-2\left(\frac{r}{R}\right)^2 + \frac{1+2k}{1+k}\right\} + \frac{R^2 u_a^2}{{D_{12}}^2} \times \left\{\frac{1}{32}\left(\frac{r}{R}\right)^8 - \frac{5}{36}\frac{1+2k}{1+k}\left(\frac{r}{R}\right)^6 + \frac{5+20k+21k^2}{24(1+k)^2} \times \left(\frac{r}{R}\right)^4 - \frac{(1+3k)(1+3k+4k^2)}{8(1+k)^3}\left(\frac{r}{R}\right)^2 + \frac{3+24k+86k^2+208k^3+251k^4}{288(1+k)^4}\right\}\right] \tag{A.25}$$

and $h_2(r, t)$ is a function such that $\lim_{t\to\infty} h_2(r, t) = 0$. From Eqs. (A.12) and (A.13) with $n = 3$, we obtain:

$$\frac{\mathrm{d}\bar{C}^{(3)}(t)}{\mathrm{d}t} = \frac{k(1+4k)}{2(1+k)^2} R^2 u_a c^{(0)} + \frac{1+10k+44k^2+122k^3+177k^4}{(1+k)^4} \times \frac{R^4 {u_a}^3}{480 {D_{12}}^2} + G_3(t) \tag{A.26}$$

where $G_3(t)$ is a function such that $\lim_{t\to\infty} G_3(t) = 0$. Therefore, Eq. (41) can be obtained.

## Appendix B. Analytical solution of the Golay's equation

The Golay's equation is classified into the telegrapher's equation, and has already been solved (refer to [39]). However, the process was not familiar to us. In this appendix, the Golay's equation is solved using a fundamental method for the linear partial differential equation.

Eq. (7) should be solved under the conditions of Eqs. (10) and (11), where $C_{app}$ is replaced by $C_G$, in the region $t > 0$ and $-\infty < z < \infty$. For convenience, we set $(1/(1+k))(m/\pi R^2) = 1$. First, we transform the equations into a normal form:

With the following variables:

$$C_G(z,t) = \exp\left(-\frac{z}{b} - \frac{2a}{b^2}t\right) F(z,t) \tag{B.1}$$

$$\xi = z - \frac{\sqrt{a^2+b^2}-a}{b}t \tag{B.2}$$

$$\chi = z + \frac{\sqrt{a^2+b^2}+a}{b}t \tag{B.3}$$

and the notation $F(z,t) = f(\xi,\chi)$, Eqs. (7), (10), and (11), respectively, become:

$$\frac{\partial^2 f}{\partial\chi^2} - \frac{\partial^2 f}{\partial\xi^2} = \alpha f \tag{B.4}$$

$$\exp\left[-\frac{1}{2b}\{(1+b^2\alpha)\xi + (1-b^2\alpha)\chi\}\right] f(\xi,\chi) = 0 \quad \text{at } (\xi,\chi) = \pm(\infty,\infty) \tag{B.5}$$

$$f(\lambda,\lambda) = \delta(\lambda) \tag{B.6}$$

where

$$\alpha = \frac{a}{b^2\sqrt{a^2+b^2}} \tag{B.6a}$$

The region $t > 0$ on the $(z,t)$-plane corresponds to the region $\chi > \xi$ on the $(\xi,\chi)$-plane.

Let $g(\xi,\chi)$ be a solution of Eq. (B.4) whose value is unity on the characteristic curves $\chi - q = \pm(\xi - p)$. Selecting the variable $\omega = \sqrt{(\chi-q)^2 - (\xi-p)^2}$ and setting $g(\xi,\chi) = G(\omega)$, we obtain:

$$\frac{d^2G}{d\omega^2} + \frac{1}{\omega}\frac{dG}{d\omega} = \alpha G \tag{B.7}$$

$$G(0) = 1 \tag{B.8}$$

The solution in the region $(\chi-q)^2 \geq (\xi-p)^2$ can be expressed using the modified Bessel function of first kind and zeroth order as:

$$G(\omega) = I_0(\sqrt{\alpha}\omega) \tag{B.9}$$

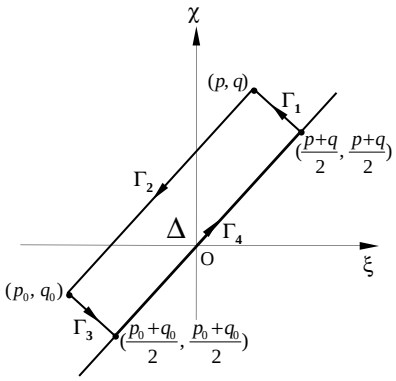


Fig. 13. Closed curve for integration.

where

$$I_0(w) = \sum_{n=0}^{\infty} \frac{1}{(n!)^2}\left(\frac{w}{2}\right)^{2n} \quad \text{for } w \geq 0 \tag{B.9a}$$

For sufficiently large $\omega$, according to the asymptotic expansion for the modified Bessel function (for example, see [27]): $I_n(w) \to \exp(w)/\sqrt{2\pi w}$ for $w \to \infty$, we obtain:

$$G(\omega) \to \frac{\exp(\sqrt{\alpha}\omega)}{\alpha^{1/4}\sqrt{2\pi\omega}} \quad \text{for } \omega \to \infty \tag{B.10}$$

$$\frac{dG(\omega)}{d\omega} \to \frac{\alpha^{1/4}\exp(\sqrt{\alpha}\omega)}{\sqrt{2\pi\omega}} \quad \text{for } \omega \to \infty \tag{B.11}$$

As shown in Fig. 13, take a point $(p,q)$ on $(\xi,\chi)$-plane (assume $p < q$).

Let $\Gamma_1$ be the directed line segment from the point $((p+q)/2, (p+q)/2)$ to the point $(p,q)$, $\Gamma_2$ the segment from $(p,q)$ to $(p_0,q_0)$ (assume $p-q = p_0-q_0$), $\Gamma_3$ the segment from $(p_0,q_0)$ to $((p_0+q_0)/2, (p_0+q_0)/2)$ and $\Gamma_4$ the segment from $((p_0+q_0)/2, (p_0+q_0)/2)$ to $((p+q)/2, (p+q)/2)$. In addition, let $\Gamma_0$ be the closed loop composed of $\Gamma_1$, $\Gamma_2$, $\Gamma_3$ and $\Gamma_4$, and $\Delta$ be the domain surrounded by $\Gamma_0$.

From Eq. (B.4) for $f(\xi,\chi)$ and $g(\xi,\chi) = G(\omega)$:

$$\frac{\partial}{\partial\xi}\left(g\frac{\partial f}{\partial\xi} - f\frac{\partial g}{\partial\xi}\right) - \frac{\partial}{\partial\chi}\left(g\frac{\partial f}{\partial\chi} - f\frac{\partial g}{\partial\chi}\right) = 0$$

Applying the Gauss' divergence theorem to the above on the domain $\Delta$:

$$\iint_{\Delta}\left\{\frac{\partial}{\partial\xi}\left(g\frac{\partial f}{\partial\xi} - f\frac{\partial g}{\partial\xi}\right) - \frac{\partial}{\partial\chi}\left(g\frac{\partial f}{\partial\chi} - f\frac{\partial g}{\partial\chi}\right)\right\} d\xi\, d\chi = \int_{\Gamma_0}\left\{g\left(\frac{\partial f}{\partial\chi}d\xi + \frac{\partial f}{\partial\xi}d\chi\right) - f\left(\frac{\partial g}{\partial\chi}d\xi + \frac{\partial g}{\partial\xi}d\chi\right)\right\} = 0$$

Dividing the path of the integral into the $\Gamma_1$, $\Gamma_2$, $\Gamma_3$ and $\Gamma_4$, we can rewrite the above equation as:

$$\int_{\Gamma_1} + \int_{\Gamma_2} + \int_{\Gamma_3} + \int_{\Gamma_4} = 0 \tag{B.12}$$

From $d\chi = -d\xi$ and $g = 1$ on $\Gamma_1$,

$$\int_{\Gamma_1} = -\int_{\Gamma_1} \mathrm{d}(fg) + 2\int_{\Gamma_1} f\,\mathrm{d}g$$
$$= -f(p,q) + f\left(\frac{p+q}{2}, \frac{p+q}{2}\right) \quad \text{(B.13)}$$

Similarly, from $\mathrm{d}\chi = \mathrm{d}\xi$ and $g = 1$ on $\Gamma_2$, $\mathrm{d}\chi = -\mathrm{d}\xi$ on $\Gamma_3$, and $\chi = \xi$ and $g((p+q)/2, (p+q)/2) = 1$ on $\Gamma_4$:

$$\int_{\Gamma_2} = -\int_{\Gamma_2} \mathrm{d}(fg) - 2\int_{\Gamma_2} f\,\mathrm{d}g = f(p_0,q_0) - f(p,q) \quad \text{(B.14)}$$

$$\int_{\Gamma 3} = f(p_0,q_0) - f\left(\frac{p_0+q_0}{2}, \frac{p_0+q_0}{2}\right) \times g\left(\frac{p_0+q_0}{2}, \frac{p_0+q_0}{2}\right) + 2\int_{\Gamma 3} f\,\mathrm{d}g \quad \text{(B.15)}$$

$$\int_{\Gamma 4} = f\left(\frac{p+q}{2}, \frac{p+q}{2}\right) - f\left(\frac{p_0+q_0}{2}, \frac{p_0+q_0}{2}\right) \times g\left(\frac{p_0+q_0}{2}, \frac{p_0+q_0}{2}\right) - 2\int_{(p_0+q_0)/2}^{(p+q)/2} f(\lambda,\lambda)\{g_\xi(\lambda,\lambda) + g_\chi(\lambda,\lambda)\}\mathrm{d}\lambda \quad \text{(B.16)}$$

When $p_0, q_0 \to -\infty$, we obtain $f(p_0,q_0) \to 0$ from Eq. (B.5) since $1 - b^2\alpha > 0$. Moreover, from Eqs. (B.5) and (B.10), we obtain $f(p_0,q_0)g(p_0,q_0) \to 0$. And

$$\int_{\Gamma 3} f\,\mathrm{d}g = \int_0^{(q-p)/2} f(p_0+\lambda, q_0-\lambda)\{g_\xi(p_0+\lambda, q_0-\lambda) + g_\chi(p_0+\lambda, q_0-\lambda)\}\mathrm{d}\lambda$$
$$= \int_0^{(q-p)/2} f(p_0+\lambda, q_0-\lambda) \times \left[\frac{\mathrm{d}G}{\mathrm{d}\omega}\frac{(\chi-q)+(\xi-p)}{\omega}\right]_{\substack{\xi=p_0+\lambda \\ \chi=q_0-\lambda}} \mathrm{d}\lambda \to 0$$

Therefore, Eq. (B.12) reduces to:

$$f(p,q) = f\left(\frac{p+q}{2}, \frac{p+q}{2}\right) - \int_{-\infty}^{(p+q)/2} f(\lambda,\lambda)\{g_\xi(\lambda,\lambda) + g_\chi(\lambda,\lambda)\}\mathrm{d}\lambda \quad \text{(B.17)}$$

From the boundary condition in Eq. (B.6), when $p+q > 0$:

$$f(p,q) = -\{g_\xi(0,0) + g_\chi(0,0)\} = \frac{q-p}{\sqrt{q^2-p^2}}\sqrt{\alpha} I_1\left(\sqrt{\alpha(q^2-p^2)}\right) \quad \text{(B.18)}$$

Exchanging the variable from $(p, q)$ to $(\xi, \chi)$, using: Eqs. (B.1)–(B.3) and multiplying $(1/(1+k))(m/(\pi R^2))$, we obtain Eq. (44) where $b$ is replaced by $b^*$. Note that $\zeta + \tau > 0$ holds for $x, t > 0$ because:

$$\zeta + \tau = \frac{x}{b} + \frac{t}{b}\left\{\frac{1+3k}{2k(1+4k)}u_a + \frac{D_{12}}{(1+k)b}\right\} \quad \text{(B.19)}$$

## References


[1] G. Taylor, Proc. R. Soc. Lond. A 219 (1953) 186.
[2] R. Aris, Proc. R. Soc. Lond. A 235 (1956) 67.
[3] J.J. Suárez, I. Medina, J.L. Bueno, Fluid Phase Equilib. 153 (1998) 167.
[4] T. Funazukuri, H. Nishiumi, in: Y. Arai, T. Sako, Y. Takebayashi (Eds.), Supercritical Fluids, Springer, Berlin, 2002, p. 182.
[5] R. Feist, G.M. Schneider, Sep. Sci. Technol. 17 (1982) 261.
[6] T.J. Bruno, J. Res. Natl. Inst. Stand. Technol. 94 (1989) 105.
[7] T.J. Bruno, in: T.J. Bruno, J.F. Ely (Eds.), Supercritical Fluid Technology, CRC Press, New York, 1991, p. 293.
[8] K.K. Liong, P.A. Wells, N.R. Foster, Ind. Eng. Chem. Res. 30 (1991) 1329.
[9] K.K. Liong, P.A. Wells, N.R. Foster, Ind. Eng. Chem. Res. 31 (1992) 390.
[10] T. Wells, N.R. Foster, R.P. Chaplin, Ind. Eng. Chem. Res. 31 (1992) 927.
[11] O.J. Catchpole, M.B. King, Ind. Eng. Chem. Res. 33 (1994) 1828.
[12] A. Akgerman, C. Erkey, M. Orejuela, Ind. Eng. Chem. Res. 35 (1996) 911.
[13] K.A. Rezaei, F. Temelli, J. Supercrit. Fluids 17 (2000) 35.
[14] H. Fu, L.A.F. Coelho, M.A. Matthews, J. Supercrit. Fluids 18 (2000) 141.
[15] H.H. Lauer, D. McManigill, R.D. Board, Anal. Chem. 55 (1983) 1370.
[16] T. Funazukuri, Y. Ishiwata, N. Wakao, AIChE J. 38 (1992) 1761.
[17] P.R. Sassiat, P. Mourier, M.H. Caude, R.H. Rosset, Anal. Chem. 59 (1987) 1164.
[18] C.C. Lai, C.S. Tan, Ind. Eng. Chem. Res. 34 (1995) 674.
[19] N. Wakao, S. Kaguei, Heat and Mass Transfer in Packed Beds, Gordon and Breach, New York, 1982, p. 17.
[20] M.J.E. Golay, Proceedings of the Second Symposium on Gas Chromatography. Academic Press, New York, 1958, p. 36.
[21] T. Funazukuri, C.Y. Kong, N. Murooka, S. Kagei, Ind. Eng. Chem. Res. 39 (2000) 4462.
[22] T. Funazukuri, C.Y. Kong, S. Kagei, Ind. Eng. Chem. Res. 41 (2002) 2812.
[23] T. Boddington, A.A. Clifford, Proc. R. Soc. Lond. A 389 (1983) 179.
[24] G. Madras, B.L. Hamilton, M.A. Matthews, Int. J. Thermophys. 17 (1996) 373.
[25] A. Alizadeh, C.A. Nieto de Castro, W.A. Wakeham, Int. J. Thermophys. 1 (1980) 243.
[26] T. Funazukuri, C.Y. Kong, S. Kagei, Int. J. Thermophys. 21 (2000) 651.
[27] M. Abramowitz, I.A. Stegun, Handbook of Mathematical Functions with Formulas, Graphs, and Mathematical Tables, Applied Mathematical Series 55, National Bureau of Standards, 1972, p. 377.
[28] T. Funazukuri, C.Y. Kong, S. Kagei, Chem. Eng. Sci., submitted for publication.
[29] T. Funazukuri, C.Y. Kong, S. Kagei, Fluid Phase Equilib., submitted for publication.
[30] R.A. Van Leer, M.E. Paulaitis, J. Chem. Eng. Data 25 (1980) 257.
[31] J. García-González, M.J. Molina, F. Rodríguez, F. Mirada, J. Chem. Eng. Data 46 (2001) 918.
[32] T. Funazukuri, C.Y. Kong, S. Kagei, Int. J. Thermophys. 21 (2000) 1279.
[33] T. Funazukuri, C.Y. Kong, S. Kagei, Fluid Phase Equilib. 194–197 (2002) 1169.
[34] X.N. Yang, L.A.F. Coelho, M.A. Matthews, Ind. Eng. Chem. Res. 39 (2000) 3059.
[35] K. Ago, H. Nishiumi, J. Chem. Eng. Jpn. 32 (1999) 563.
[36] H. Nishiumi, M. Fujita, K. Agou, Fluid Phase Equilib. 117 (1996) 35.
[37] J.M.H. Levelt Sengers, U.K. Deiters, U. Klask, P. Swidersky, G.M. Schneider, Int. J. Thermophys. 14 (1993) 893.
[38] A.A. Clifford, S.E. Coleby, Proc. R. Soc. Lond. A 433 (1991) 63.
[39] M.J.E. Golay, Anal. Chem. 29 (1957) 928.